Separation Science and Technology
Publication details, including instructions for authors and subscription information:
http://www.informaworld.com/smpp/title~content=t713708471

Hyperbolic-Tangent Model Analysis of Permeate Flux for Ultrafiltration in Hollow-Fiber Modules by Momentum Balance

H. M. Yeh[a]; C. D. Ho[a]; S. Y. Lee[a]
[a] Department of Chemical and Materials Engineering, Tamkang University, Tamsui, Taiwan

To cite this Article Yeh, H. M. , Ho, C. D. and Lee, S. Y.(2008) 'Hyperbolic-Tangent Model Analysis of Permeate Flux for Ultrafiltration in Hollow-Fiber Modules by Momentum Balance', Separation Science and Technology, 43: 2, 245 — 258
To link to this Article: DOI: 10.1080/01496390701787420
URL: http://dx.doi.org/10.1080/01496390701787420

Separation Science and Technology, 43: 245–258, 2008

ISSN 0149-6395 print/1520-5754 online
DOI: 10.1080/01496390701787420

Hyperbolic-Tangent Model Analysis of Permeate Flux for Ultrafiltration in Hollow-Fiber Modules by Momentum Balance

H. M. Yeh, C. D. Ho, and S. Y. Lee

Department of Chemical and Materials Engineering, Tamkang University, Tamsui, Taiwan

Abstract: The predicting equation for the permeate flux of membrane ultrafiltration in hollow-fiber modules, was derived from the complete momentum balance coupled with the application of hyperbolic-tangent model. The correlation predictions obtained in present modeling study are based on the consideration of the effect of the loss of momentum transfer due to convection. It is found that the hyperbolic-tangent model analysis for permeate flux confirms well with the ultrafiltration of polyvinyl alcohol aqueous solution in hollow fiber modules.

Keywords: Ultrafiltration, hyperbolic-tangent model, momentum balance

INTRODUCTION

The main application of ultrafiltration is the separation of fairly large molecules. Nowadays, it is applied in a wide variety of fields, from the chemical industry (including eletrocoat paint recovery, latex processing, textile size recovery, and recovery of lubricating oil), to medical applications (such as kidney dialysis operation), and even to biotechnology (including concentration of milk, egg white, juice, pectin and sugar, and recovery of protein from cheese whey, animal blood, gelatin, and glue) (1–3).

Membrane UF process is usually analyzed by the gel polarization model (4–10), the osmotic pressure model (11–19), and the resistance-in-series

Received 13 June 2007, Accepted 16 October 2007

Address correspondence to C. D. Ho, Department of Chemical and Materials Engineering, Tamkang University, Tamsui 251, Taiwan. Tel.: +886-2-26215656; Fax: +886-2-26209887; E-mail: cdho@mail.tku.edu.tw

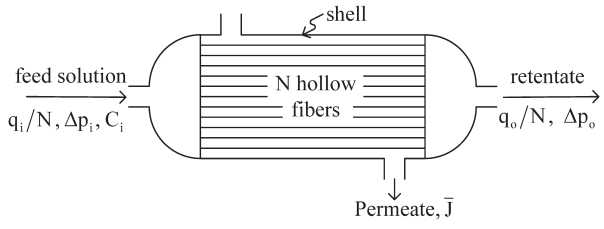

Figure 1. Hollow-fiber ultrafilter.

model (20–22). In the gel polarization model, the permeate flux is reduced by the hydraulic resistance of the gel layer. In the osmotic pressure model, the permeate flux reduction results from the decrease in effective transmembrane pressure that occurs as the osmotic pressure of the retentate increases. In the resistance-in-series model, the permeate flux decreases due to the resistances caused by fouling or solute adsorption and concentration polarization (CP). Recently, Song, and Elimelech (23) developed the fundamental theory and methodology providing a solid basis for the study of limiting flux in UF. Later, a mechanistic model for predicting the limiting flux in UF was also developed (24). In this study, the hyperbolic-tangent model for predicting the permeate flux of UF in hollow-fiber modules is introduced, and the incline of the transmembrane pressure due to the momentum loss by convection is taken into consideration.

THEORY

Consider a hollow-fiber module with N fibers of same size, in which the membrane is formed on the inside of N tiny porous tubes that are then bundled and potted into a tube-and-shell arrangement, as shown in Fig. 1, while Fig. 2 shows the flows and fluxes in the fiber tube of radius r_m and length L.

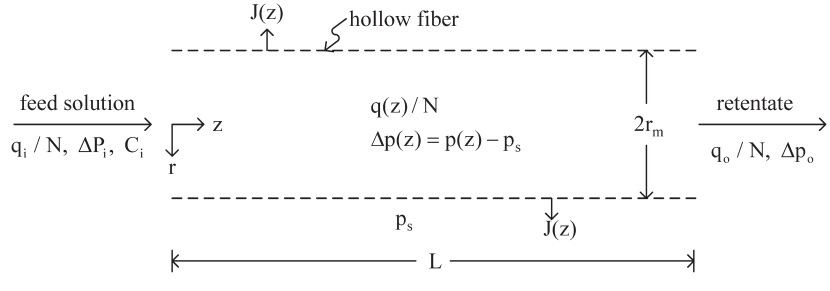

Figure 2. Flows and fluxes in a hollow-fiber for ultrafiltration.

Mass Balance

Let $q(z)/N$ be the volumetric flow rate of solution in a hollow-fiber and J be the permeate flux by ultrafiltration. Then, a mass balance over a slice dz of the fiber gives

$$\frac{d(q/N)}{dz} = -2\pi r_m J \tag{1}$$

Momentum Balance

The problem dealing with the pressure distribution can be approached by setting up momentum balance within the differential length dz of a hollow-fiber. For steady-state operation (25)

$$\frac{d}{dz}(\rho u_b^2) + \frac{d}{dz}(\Delta p) + \frac{\tau_s(2\pi r_m)}{\pi r_m^2} = 0 \tag{2}$$

where $\Delta p(=p - p_s)$ denotes the transmembrane pressure, and $p(z)$ and p_s are the pressures in the fiber tube and the shell sides, respectively, while the shear stress τ_s relates to the friction factor f and bulk velocity of fluid u_b as $\tau_s = (\rho u_b^2/2)f$. For laminar flow, $f = 16/(2r_m u_b \rho/\mu)$, and for flow in a tube, $(q/N) = \pi r_m^2 u_b$, the above equation can be rewritten as:

$$\frac{\rho}{\pi^2 r_m^4}\frac{d(q/N)^2}{dz} + \frac{d\Delta p}{dz} + \frac{8\mu(q/N)}{\pi r_m^4} = 0 \tag{3}$$

The three terms in the left-hand side of Eq. (3) denote, respectively, the rate of momentum transfer by convection, the pressure force, and the rate of momentum by viscous transfer.

Hyperbolic-Tangent Model

Ultrafiltration is a pressure-driven membrane separation process. The working pressure, usually applied to the solution in the range of 100–1000 kPa, provides the driving potential to force the solvent or the solute consisting of smaller molecules to flow through the membrane while the larger molecules are rejected by the membrane. For a small applied pressure, the permeate flux through a membrane is observed to be proportional to the applied pressure. However, as the pressure is increased, the flux begins to drop below that which would result from a linear-pressure behavior. Eventually, the limiting flux is reached where any further pressure increase no longer results in any increase in flux. Accordingly, the following relations between

permeate flux J(z) and transmembrane pressure Δp are reached:

$$J = 0, \quad \text{for } \Delta p = 0 \tag{4}$$

$$J = (\text{constant})\Delta p, \quad \text{for small } \Delta p \tag{5}$$

$$J = J_{lim}, \quad \text{as } \Delta p \to \infty \text{ (or large enough)} \tag{6}$$

Therefore, the hyperbolic-tangent model is thus introduced and may be expressed as

$$V = \tanh(\beta \Delta P) \tag{7}$$

in which

$$V = J/J_{lim} \tag{8}$$

$$\Delta P = \Delta p/\Delta p_i \tag{9}$$

$$\beta = (\Delta p_i)/(R \cdot J_{lim}) \tag{10}$$

where Δp_i is the transmembrane pressure at the inlet and R denotes the total resistances of ultrafiltration due to the intrinsic resistance, concentration polarization and fouling. J_{lim} and R can be determined experimentally. It is easy to check that Eq. (7) satisfies Eqs. (4) and (6), as well as Eq. (5) if we rewrite Eq. (7) as

$$V = \beta(\Delta P) - \frac{\beta^3(\Delta P)^3}{3!} + \frac{2\beta^5(\Delta P)^5}{15} - \cdots\cdots \tag{11}$$

Incline of Transmembrane Pressure

Define the following dimensionless groups with fiber length L:

$$Q = \frac{8\mu L(q/N)}{\pi r_m^4 \Delta p_i} \tag{12}$$

$$\alpha = \frac{16\mu L^2 J_{lim}}{r_m^3(\Delta p_i)} \tag{13}$$

$$\gamma = \frac{\rho r_m^4(\Delta p_i)}{64\mu^2 L^2} \tag{14}$$

$$Z = \frac{z}{L} \tag{15}$$

With the use of above relations, Eqs. (1) and (3) may be rewritten as

$$\frac{dQ}{dz} = -\alpha V \tag{16}$$

$$\gamma \frac{dQ^2}{dZ} + \frac{d\Delta P}{dZ} + Q = 0 \tag{17}$$

Substitution of Eq. (7) into Eq. (16) yields

$$\frac{dQ}{dZ} = -\alpha \tanh(\beta \Delta P) \tag{18}$$

The flow rate of solution declines along the fiber tube due to membrane ultrafiltration and thus, solvent is permeated through the porous tube wall by transmembrane pressure. Since the permeate rate is very small compared with the volume flow rate ($q/N >> 2\pi r_m \int_0^L J dz$), we may assume in Eqs. (1) and (18) that q/N declines slightly and linearly along the hollow-fiber by approximately setting $J = J(0)$ and $\Delta p = \Delta p_i (\Delta P = 1)$ for mathematical simplicity. Accordingly, the integration of Eq. (18) from $Z = 0$ ($Q = Q_i$, i.e. $q = q_i$) to $Z = Z$ results in

$$Q = Q_i - \alpha \int_0^Z (\tanh \beta) dZ = Q_i - \alpha (\tanh \beta) Z \tag{19}$$

Substituting Eq. (19) into Eq. (17) and integrating from $Z = 0$ ($\Delta P = 1$) to Z, one obtains

$$\Delta P = 1 - [1 - 2\alpha\gamma(\tanh \beta)][Q_i Z - (\alpha/2)(\tanh \beta) Z^2] \tag{20}$$

or

$$\Delta P = 1 + (\alpha/2)(\tanh \beta)[1 - 2\alpha\gamma(\tanh \beta)][Z^2 - 2\{Q_i/\alpha(\tanh \beta)\}Z] \tag{21}$$

Average Permeate Flux

The average permeate flux can be obtained from

$$\bar{J} = \frac{1}{L} \int_0^L J(z) dz \tag{22}$$

or, in dimensionless form

$$\bar{V} = \int_0^1 V(Z) dZ \tag{23}$$

where

$$\bar{V} = \bar{J}/J_{lim} \tag{24}$$

Substituting Eqs. (7) and (21) into Eq. (23), we have

$$\bar{V} = \int_0^1 (\tanh \beta)[1 - A(Z - BZ^2)] dZ \tag{25}$$

where

$$A = Q_i[1 - (2\alpha\gamma)\tanh\beta] \tag{26}$$

$$B = (\alpha/2Q_i)\tanh\beta \tag{27}$$

RESULTS AND DISCUSSION

Previous Works

The theoretical predictions of average permeate flux $\bar{J}$ obtained in the previous works (22, 26, 27), in which the rate of momentum transfer by convection along the fiber tube was neglected, i.e. $\gamma = 0$ in Eq. (17), will be improved in present study. The Amicon model H1P 30-20 hollow-fiber cartridges ($r_m = 2.5 \times 10^{-4}$ m, $L = 0.153$ m, $N = 250$, $MWCO = 30{,}000$) made of polysulfone were used for ultrafiltration of aqueous solutions of dextran T500 (22) (Pharmacia Co., $M_n = 170{,}300$), polyvinylpyrrolidone (26) (PVP-360, Sigma Co., $M_n = 360{,}000$), and polyvinyl alcohol (27) (PVA, Sigma Co., $M_n = 320{,}000$). The experiments were conducted at 25°C and the duration of each experimental run is about 30∼120 minutes after the pseudo steady-state was reached. The reason why we choose the above aqueous solutions is that the experimental data of these three systems for comparing with correlation predictions are readily available in the results of previous works, in which the theoretical treatments should be modified. Some of the experimental results of average permeate fluxes for these three aqueous solutions are presented, respectively, in Figs. 3 and 4, Figs. 5 and 6, and Figs. 7 and 8.

Determination of J_{lim} and R

It was pointed out that $(1/\bar{J})_{exp}$ vs. $(1/\overline{\Delta p})_{exp}$ is a straight line (20, 28, 29). Accordingly, when the abscissa $(1/\overline{\Delta p})_{exp}$ is zero, i.e., $(\overline{\Delta p})_{exp} \to \infty$, the intersection of the straight line at the ordinate will be $(1/J_{lim})$, as indicated by Eq. (6). Further, Eq. (7) may be rewritten as

$$\tanh(\bar{J}/J_{lim})_{exp} = (\overline{\Delta p})_{exp}/RJ_{lim} \tag{28}$$

Consequently, the straight-line plot of $\tanh^{-1}(\bar{J}/J_{lim})_{exp}$ vs. $(\overline{\Delta p})_{exp}$ will result in the slope of $1/(R \cdot J_{lim})$ as well as R.

The correlation equations of J_{lim} (m s^{-1}) and R (Pa s m^{-1}) were derived with the use of the experimental data of J_{lim} and R and the method of least

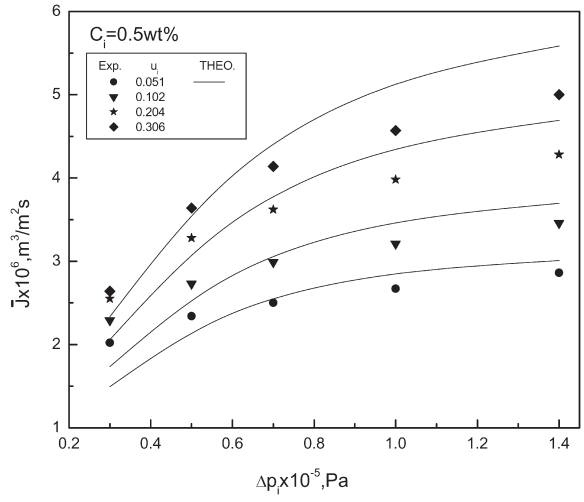

Figure 3. Average permeate flux for dextran T500 aqueous solution with $C_i = 0.5$ wt%.

square (28, 29). They are

$$J_{lim} \times 10^5 = 4.02 u_i^{1.266} C_i^{-1.783} \tag{29}$$

$$R \times 10^{-9} = 1.38 u_i^{-1.14} C_i^{1.766} \tag{30}$$

$$\mu \times 10^3 = 0.894 \exp(0.408 C_i)^{[22]} \tag{31}$$

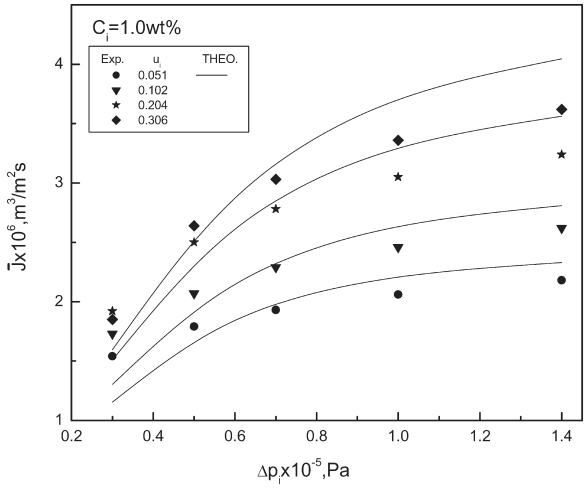

Figure 4. Average permeate flux for dextran T500 aqueous solution with $C_i = 1.0$ wt%.

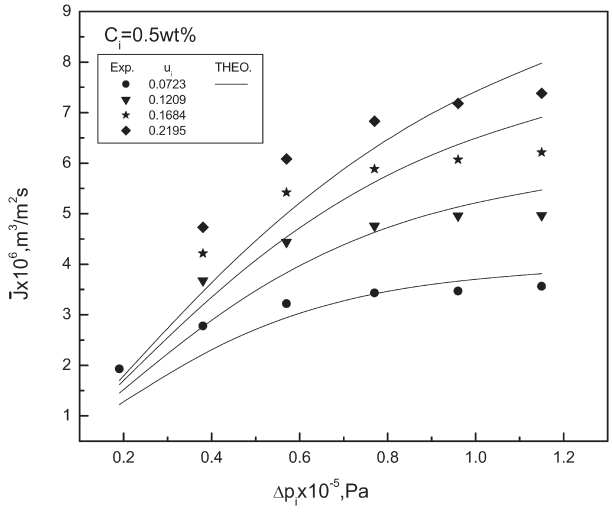

Figure 5. Average permeate flux for PVP-360 aqueous solution with $C_i = 0.5$ wt%.

for dextran T500,

$$J_{lim} \times 10^5 = 2.54 u_i^{0.765} C_i^{-0.3} \tag{32}$$

$$R \times 10^{-9} = 5.25 u_i^{-0.287} C_i^{0.204} \tag{33}$$

$$\mu \times 10^3 = 0.894 \exp(0.875 C_i)^{[26]} \tag{34}$$

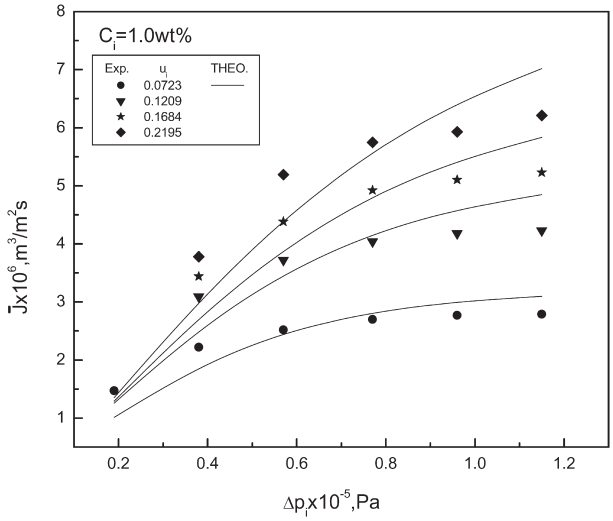

Figure 6. Average permeate flux for PVP-360 aqueous solution with $C_i = 1.0$ wt%.

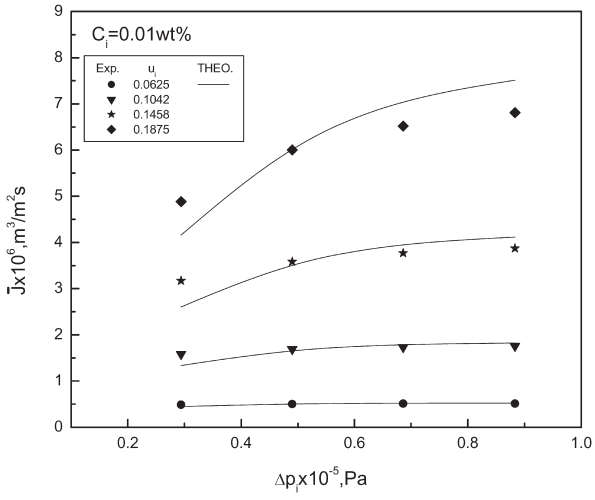

Figure 7. Average permeate flux for PVA aqueous solution with $C_i = 0.01$ wt%.

for PVP-360, and

$$J_{lim} \times 10^5 = 1.29 u_i^{2.367} C_i^{-0.247} \tag{35}$$

$$R \times 10^{-9} = 7.39 u_i^{-1.816} C_i^{0.334} \tag{36}$$

$$\mu \times 10^3 = 3.2^{[27]} \tag{37}$$

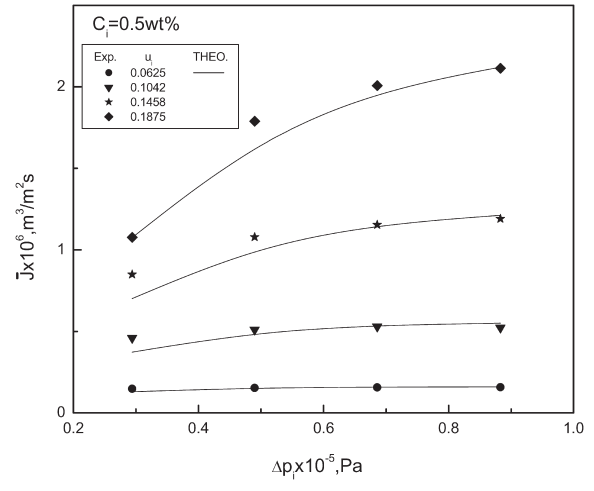

Figure 8. Average permeate flux for PVA aqueous solution with $C_i = 0.5$ wt%.

for PVA aqueous solution. It is noted that for the use of calculating the permeate flux, the correlation equations of viscosity μ(Pa s) are also provided in Eqs. (31), (34), and (37).

Correlation Predictions

The correlation predictions of average permeate flux, $\bar{J}$, under various inlet transmembrane pressures, Δp_i, feed concentrations, C_i, and fluid velocities, u_i, were calculated from Eqs. (24) and (25) by numerical integration coupled with the use of Eqs. (29)–(37). The calculated results are plotted and compared with the experimental data, as shown in Figs. 3–8. As seen in Figs. 7 and 8, the correlation results confirm well with the experimental data of PVA aqueous solution, while those for the aqueous solutions of dextran T500 and PVP-360 qualitatively confirm with the experimental data, as shown in Figs. 3–6. Nevertheless, the deviations between the theoretical predictions and the experimental results are small for dextran T500 solution under the middle range of transmembrane pressures ($\Delta P_i = 0.4 \times 10^5 \sim 0.7 \times 10^5$ Pa), and for PVP-360 solution under higher transmembrane pressures. The deviation for dextran T500 system may lower to 3% in the case of $\Delta P_i = 0.7 \times 10^5$ Pa and $C_i = 0.5$ wt%, while that for PVP-360 system is lower than 5% at the condition of $\Delta P_i = 0.96 \times 10^5$ Pa and $C_i = 0.5$ wt%. As a whole, the deviation turns smaller as the fluid velocity decreases, while it diverges when the transmembrane pressure decreases. This will be explained as follows. One of the essential behaviors of ultrafiltration is that $J = (\text{constant})\Delta p$ for small Δp, as mentioned in Eq. (5). However, the present model simulates that $(J/J_{lim}) \approx \beta(\Delta p/\Delta p_i)$ for small Δp but actually $(J/J_{lim}) - \beta(\Delta p/\Delta p_i) < 0$, as shown in Eq. (11). Accordingly, the correlation predictions are smaller than the experimental results at low transmembrane pressure.

The accuracy of the experimental permeate flux for dextran T500, PVP-360 and PVA under varied feed solution concentration and inlet fluid velocity in the hollow fiber may be calculated using the following definition

$$\text{Err}(\%) = \frac{1}{M}\sum_{j=1}^{M}\frac{|J_j^{\text{Theo.}} - J_j^{\text{Exp.}}|}{J_j^{\text{Exp.}}} \times 100\% \tag{38}$$

The average percentage error of the experimental measurements in Figs. 3–8 is $4.94\% < \text{Err}(\%) < 10.46\%$. It is seen the error analysis of experimental runs for dextran T500, PVP-360 and PVA in Figs. 3–8 that the agreement between the experimental data and the correlation results is fairly good. It is concluded that the hyperbolic-tangent model is better suitable for the permeation analysis of ultrafiltration of polyvinyl alcohol aqueous solution in a hollow fiber cartridge.

The assumption of laminar flow is easy to check by the maximum value of Reynolds number with $u_i = 0.306\ m/s$, $C_i = 0.1$ wt%, and $\bar{J} = 9.08 \times 10^{-6}\ m^3/m^2 \cdot s$ in Figs. 3–8 as

$$(Re)_{max} = \frac{2r_m u_i \rho}{\mu} = \frac{2(2.5 \times 10^{-4})(0.306)(1000)}{0.894 \times 10^{-3} e^{0.408(0.1)}}$$
$$= 164 < 2100$$

Therefore, the assumption of laminar flow is acceptable for the system of present interest. Further, since

$$q_i/N = \pi r_m^2 u_i = \pi(2.5 \times 10^{-4})^2(0.306) = 6 \times 10^{-8} m^3/s$$
$$2\pi r_m L\bar{J} = 2\pi(2.5 \times 10^{-4})(0.153)(9.08 \times 10^{-6}) = 2.18 \times 10^{-9} m^3/s$$
$$q_o/N = q_i/N - 2\pi r_m L\bar{J} = 5.78 \times 10^{-8} m^3/s$$

and

$$\frac{(q_i - q_o)/N}{q_i/N} = \frac{2.18 \times 10^{-9}}{6 \times 10^{-8}} = 3.6\%$$

Consequently, the assumption that q/N declines slightly and linearly is acceptable.

CONCLUSION

The predicting equation, Eq. (25), for the average permeate fluxes of membrane ultrafiltration in hollow-fiber modules, was derived by the hyperbolic-tangent model coupled with the application of complete momentum balance, in which the momentum transfer by convection (fluid motion) was taken into consideration. It is found that the correlation predictions of permeate flux obtained in present study are more accurate than those obtained in the previous work (22, 26, 27), in which the momentum balances were taken inaccurately by simply applying Hagen-Poiseuille theory without the considerations of the effects of the permeate flux loss and the loss of momentum flux due to fluid motion, on overall momentum balance.

As mentioned earlier, the hyperbolic-tangent model satisfies the three essential conditions of membrane ultrafiltration, Eqs. (4)–(6). Therefore, the present model easily describes the relationships of permeate flux with operating and design parameters. It is confirmed that this model predicts well the permeate flux for ultrafiltration of PVA aqueous solution in a hollow fiber module. We believe that hyperbolic-tangent model may be preferably suitable for some membrane ultrafiltration systems including systems with different kinds of feed solutions, different materials of membrane tubes, and various design and operating conditions.

NOMENCLATURE

C_i	concentration of feed solution (wt%)
f	friction factor
J	permeate flux of solution ($m^3\ m^{-2}\ s^{-1}$)
J_{lim}	limiting flux ($m^3\ m^{-2}\ s^{-1}$)
L	fffective length of hollow fiber (m)
M	the number of experimental measurements
N	number of hollow fibers in a membrane module
p	pressure distribution on the tube side (Pa)
p_s	uniform permeate pressure on the shell side (Pa)
Δp	transmembrane pressure, $p - p_s$ (Pa)
ΔP	dimensionless transmembrane pressure, $\Delta p/\Delta p_i$
q	volume flow rate in a hollow-fiber module ($m^3\ s^{-1}$)
Q	dimensionless flow rate, $8\ \mu L(q/N)/(\pi r_m^4 \Delta P_i)$, defined by Eq. (12)
r_m	inside radius of hollow-fiber (m)
R	total resistances (Pa s m^{-1})
u	fluid velocity in the hollow fiber, $q/N(\pi r_m^2)$(m s^{-1})
V	dimensionless permeate flux, J/J_{lim}, defined by Eq. (8)
z	axial coordinate (m)
Z	dimensionless axial coordinate, z/L

Greek Letters

α	dimensionless group, $16\ \mu L^2 J_{lim}/[r_m^3\ (\Delta P_i)]$, defined by Eq. (13)
β	dimensionless group, $\Delta P_i/(RJ_{lim})$, defined by Eq. (10)
γ	dimensionless group, $\rho r_m^4\ (\Delta P_i)/(64\mu^2 L^2)$, defined by Eq. (14)
μ	viscosity of solution (Pa s)
τ_s	shear stress (Pa)

Superscripts

Exp.	the experimental measurements
Theo.	the correlation results
−	average value

Subscripts

i	at the inlet
o	at the outlet
b	average

ACKNOWLEDGMENTS

The authors wish to express their thanks to the National Science Council of ROC for financial aid with the Grant No. NSC 94-2214-E-02-005.

REFERENCES

1. Ho, W.S.W. and Sirkar, K.K. (1992) *Membrane Handbook*; Chapman and Hall: New York.
2. Schweitzer, P.A. (1979) *Handbook of Separation Techniques for Chemical Engineers*; McGraw-Hill: New York.
3. Cheryan, M. (1986) *Ultrafiltration Handbook*; Technomic Publiching Co. Inc.: Lancaster, Pennsylvania.
4. Nokao, S., Nomura, T., and Kimura, S. (1979) Characteristics of macromolecular gel layer formed on ultrafiltration tubular membrane. *AIChE J.*, 25: 615.
5. Fane, A.G., Fell, C.J. D., and Waters, A.G. (1981) The relationship between membrane surface pore characteristics and flux for ultrafiltration membranes. *J. Member. Sci.*, 9: 245.
6. Filnn, J.E. (1970) *Membrane Science and Technology*; Plenum Press: New York.
7. Porter, M.C. (1972) Concentration polarization with membrane ultrafiltration. *Ind. Eng. Chem. Proc. Res. Dev.*, 11: 234.
8. Grieves, R.B., Bhattacharyya, D., Schomp, W.G., and Bewley, J.L. (1973) Membrane ultrafiltration of a nonionic surfactant. *AIChE J.*, 19: 766.
9. Shen, J.J. S. and Probstein, R.F. (1977) On the prediction of limiting flux in laminar ultrafiltration of macromolecular solutions. *Ind. Eng. Chem. Fundam.*, 16: 459.
10. Fane, A.G. (1984) Ultrafiltration of suspensions. *J. Membr. Sci.*, 20: 249.
11. Clifton, M.J., Abidine, N., Aptel, P., and Sanchez, V. (1984) Growth of the polarization layer in ultrafiltration with hollow-fiber membranes. *J. Membr. Sci.*, 21: 233.
12. Wijmans, J.G., Nakao, S., and Smolders, C.A. (1984) Flux limitation in ultrafiltration: osmotic pressure model and gel layer model. *J. Membr. Sci.*, 20: 115.
13. Kozinki, A.A. and Lightfoot, E.N. (1972) Protein ultrafiltration: a general example of boundary layer filtration. *AIChE J.*, 18: 1030.
14. Leung, W. and Probstein, R.F. (1979) Low polarization in laminar ultrafiltration of macromolecular solutions. *Ind. Eng. Chem. Fundam.*, 18: 274.
15. Wendt, R.P., Klein, E., Holland, F.F., and Eberle, K.E. (1981) Hollow fiber ultrafiltration of calf serum and albumin in the pregel uniform-wall-flux region. *Chem. Eng. Commun.*, 8: 251.
16. Nakao, S. and Kimura, S. (1982) Model of membrane transport phenomena and their applications for ultrafilration data. *J. Chem. Eng. Jpn.*, 15: 200.
17. Kleinstreuer, C. and Paller, M.S. (1983) Laminar dilute suspension flows in plate-and-frame ultrafiltration units. *AIChE J.*, 29: 529.
18. Ma, R.P., Gooding, C.H., and Alexander, W.K. (1985) A dynamic model for low-pressure, hollow-fiber ultrafiltration. *AIChE J.*, 31: 1782.
19. Nabetani, H., Nakajima, M., Watanable, A., Nakao, S., and Kumura, S. (1990) Effects of osmotic pressure and adsorption on ultrafiltration of ovalbumin. *AIChE J.*, 36: 907.

20. Chiang, B.H. and Cheryan, M. (1986) Ultrafiltration on skim milk in hollow fibers. *J. Food Sci.*, 51: 340.
21. Assadi, M. and White, D.A. (1992) A model for determining the steady state flux of inorganic microfiltration membrane. *Chem. Eng. J.*, 48: 11.
22. Yeh, H.M. and Cheng, T.W. (1993) Resistance-in-series for membrane ultrafiltration in hollow fiber of tube-and-shell arrangement. *Sep. Sci. Technol.*, 28: 1341.
23. Song, L. and Elimelech, M. (1995) Theory of concentration polarization in crossflow filtration. *J. Chem. Soc. Faraday Trans.*, 91: 3389.
24. Song, L. (1998) A new model for the calculation of the limiting flux in ultrafiltration. *J. Membr. Sci.*, 144: 173.
25. Bird, R.B.; Stewart W. E. and Lightfoot, E.N. (1971) *Transport Phenomena*; Wiley: New York.
26. Yeh, H.M. and Cheng, T.W. (1998) Permeate flux behaviors under various pressure declines in membrane ultrafiltration module. *Chem. Eng. Commum.*, 170: 185.
27. Yeh, H.M., Chen, T.W., and Yeh, Y.J. (2000) Sizing agent recovery by membrane ultrsfiltration in hollow-fiber modules. *Chem. Eng. Commum.*, 177: 204.
28. Yeh, H.M. and Wu, H.H. (1997) Membrane ultrafiltration in combined hollow-fiber module systems. *J. Membr. Sci.*, 124: 93.
29. Yeh, H.M. and Tsai, J.W. (1998) Membrane ultrafiltration in multipass hollow-fiber modules. *J. Membr. Sci.*, 142: 61.
30. Cheng, T.W. (1992) *A Study on the Hollow-Fiber Membrane Ultrafiltration*; Ph.D Diss; National Taiwan University: Taipei, Taiwan.